Stable polyoxometalate insertion within the mesoporous metal organic framework MIL-100(Fe)†

Romain Canioni,[a] Catherine Roch-Marchal,*[a] Francis Sécheresse,[a] Patricia Horcajada,*[a] Christian Serre,[a] Menaschi Hardi-Dan,[a] Gérard Férey,[a] Jean-Marc Grenèche,[b] Frédéric Lefebvre,[c] Jong-San Chang,[d] Young-Kyu Hwang,[d] Oleg Lebedev,[e] Stuart Turner[f] and Gustaaf Van Tendeloo[f]

Received 23rd July 2010, Accepted 5th October 2010
DOI: 10.1039/c0jm02381g

Successful encapsulation of polyoxometalate (POM) within the framework of a mesoporous iron trimesate MIL-100(Fe) sample has been achieved by direct hydrothermal synthesis in the absence of fluorine. XRPD, ^{31}P MAS NMR, IR, EELS, TEM and ^{57}Fe Mössbauer spectrometry corroborate the insertion of POM within the cavities of the MOF. The experimental Mo/Fe ratio is 0.95, in agreement with the maximum theoretical amount of POM loaded within the pores of MIL-100(Fe), based on steric hindrance considerations. The POM-MIL-100(Fe) sample exhibits a pore volume of 0.373 cm^3 g^{-1} and a BET surface area close to 1000 m^2 g^{-1}, indicating that small gas molecules can easily diffuse inside the cavities despite the presence of heavy phosphomolybdates. These latter contribute to the decrease in the overall surface area, due to the increase in molar weight, by 65%. Moreover, the resulting Keggin containing MIL-100(Fe) solid is stable in aqueous solution with no POM leaching even after more than 2 months. In addition, no exchange of the Keggin anions by tetrabutylammonium perchlorate in organic media has been observed.

Introduction

The numerous applications of polyoxometalates (POM) in acid and oxidation catalysis have recently attracted great attention.[1] However, their applications are limited by their low specific surface area, low stability under catalytic conditions and high solubility in aqueous solution. One of the strategies to overcome these drawbacks consists of their encapsulation within porous solid matrixes. Recently, this strategy was applied to a few selected large pores Metal Organic Frameworks (MOFs),[2] crystalline solids that combine a versatile and easily tunable hybrid framework and an important ordered porosity.[3,4]

Recently, studies of many POM based MOFs have been reported,[3] built up from the association (direct or post-synthesis) of POMs, mono- or divalent cations (Ag, Cu, Zn…) and different types of linkers (carboxylates, pyrazolates, bipyridine…). POMs are either encapsulated within the pores or are directly part of the framework. However, very little information is reported on their stability (leaching) and/or their real accessible porosity. An interesting case concerns the direct synthesis of the highly porous copper trimesate HKUST-1 loaded with POM moieties,[5] with however a low resulting (Langmuir) surface area, close to 460 m^2 g^{-1}.[1] The authors reported interesting catalytic properties but as it is well established that copper carboxylate based MOFs dissolve in water, this might rule out their practical use for liquid phase applications.[6] As a result, most POM-loaded MOFs reported so far probably lack sufficient thermal and chemical stability to prevent leaching and allow an appropriate diffusion of catalytic reactants. In consequence, there is still a strong need to develop new POM-MOF stable supports.

Some of us reported recently the mesoporous metal polycarboxylates with a zeotype architecture denoted MIL-100[7] or MIL-101[4] (MIL stands for Material from Institut Lavoisier). Both solids are built up from iron or chromium oxo-centred trimers connected by polycarboxylate linkers resulting in hybrid supertetrahedra, further delimiting two sets of mesoporous cages (Fig. 1).[8] As a result, MIL-100(Fe) and MIL-101(Cr) exhibit upon dehydration an important porosity (for MIL-100(Fe, Cr), S_{BET} = 1900 m^2 g^{-1}, V_p = 1.2 cm^3 g^{-1}, for MIL-101(Cr), S_{BET} = 3200–4200 m^2 g^{-1}, V_p = 1.6–2.3 cm^3 g^{-1}) with the presence of a significant amount of accessible Lewis acid metal sites.[9,10] In the case of MIL-101(Cr), the larger mesoporous cages (34 Å) are accessible through large microporous windows (16 Å), allowing an easy post-synthesis loading of POMs within these pores.[4] Several studies have reported the loading of various types of metal substituted POMs in MIL-101(Cr), including details on their catalytic properties as well as insights into their stability.[5,11,12] However, the high toxicity of chromium makes it necessary to develop loading

[a]*I.L.V., Institut Lavoisier de Versailles, UMR 8180, Université de Versailles-St Quentin en Yvelines, 45 Avenue des États-Unis, 78035 Versailles Cedex, France. E-mail: Roch@chimie.uvsq.fr; horcajada@chimie.uvsq.fr.; Fax: +33(1)39254388; Tel: +33(1)39254381*
[b]*Laboratoire de Physique de l'Etat Condensé LPEC, UMR CNRS 6087, Université du Maine, Avenue Olivier Messiaen, 72085 LE MANS Cedex France*
[c]*Laboratoire C2P2, Equipe de Chimie Organométallique de Surface, LCOMS, UMR 526, CPE Lyon, 43 Bd du 11 Novembre 1918, F-69616 Villeurbanne cedex, France*
[d]*Catalysis Center for Molecular Engineering, Korea Research Institute of Chemical Technology (KRICT), P.O. Box 107, Yuseong, Daejeon, 305600, Republic of Korea*
[e]*Laboratoire CRISMAT, UMR 6508 CNRS/ENSICAEN, 6 bd du Maréchal Juin, F-14050 CAEN, Cedex 4 - France*
[f]*Electron Microscopy for Materials Research (EMAT), University of Antwerp, Groenenborgerlaan 171, B2020 Antwerpen, Belgium*

† Electronic supplementary information (ESI) available: Elemental analysis, schematic representations of the structure, X-ray thermodiffraction patterns, X-ray diffraction patterns of Na_2HPMo_{12}/MIL-100(Fe)noF and nitrogen isotherms and porous distribution of Na_2HPMo_{12}/MIL-100(Fe)noF. See DOI: 10.1039/c0jm02381g

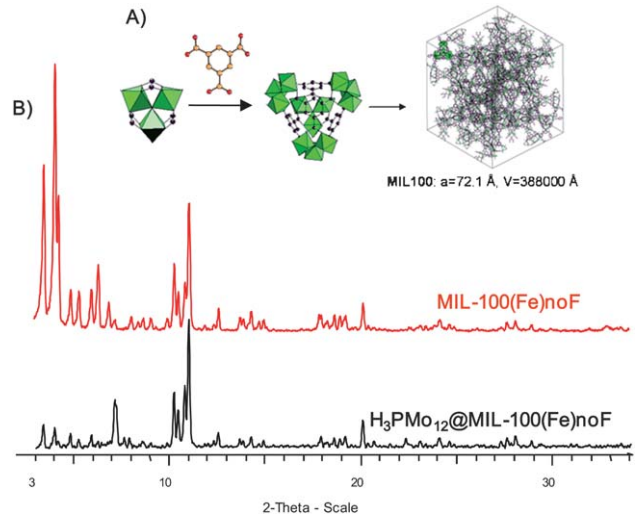

Fig. 1 A) Schematic view of MIL-100(Fe): trimers of iron octahedra and trimesic acid (left), the resulting hybrid supertetrahedra (centre) and one unit cell (right). Ball and stick view (Fe octahedra: grey, O: black, C: grey). B) XRPD patterns of MIL-100(Fe)noF and H_3PMo_{12}@MIL-100(Fe)noF.

methods of POMs in the less toxic iron based MOFs. In the case of MIL-100(Fe) or $Fe^{III}_3O(H_2O)_2(F)\{C_6H_3(CO_2)_3\}_2 \cdot nH_2O$ (n = 14.5),[8] the mesoporous cages of *ca.* 25 and 29 Å free diameters are accessible through pentagonal and hexagonal windows of free diameter close to 5.5 and 8.6 Å, respectively, which rules out the possibility of a post-synthesis encapsulation of POMs within its pores. On the other hand, if one could synthesise directly a POM-loaded MIL100(Fe) solid, this would decrease the risk of any catalyst leaching. In addition to its low toxicity, MIL-100(Fe) fulfils many of the conditions required for a POM support: i) cheap composition, ii) high thermal (270 °C under air) and hydrothermal stability, and iii) 3D mesoporous system suitable for high POM loading capacities as well as easier diffusion of the gaseous reactants.

Here, we propose a synthesis method for the encapsulation within the pores of MIL-100(Fe) matrices of a model oxidative catalyst phosphomolybdate $[PMo_{12}O_{40}]^{3-}$ Keggin heteropolyanion. This POM is hydrothermally stable and possesses a 13 Å van der Waals diameter.[13] Phosphomolybdates are also oxidative heterogeneous catalysts in gas or liquid phases,[14] and can activate C–H bonds in aromatic and alkyl aromatic compounds and oxygenate such substrates according to a Mars–van Krevelen-type mechanism in both phases[15]

Different synthetic methods have been investigated: (i) direct synthesis of MIL-100(Fe) in the presence of heteropolyacid; (ii) direct synthesis of heteropolyanion inside the cages of formed MIL-100(Fe) and (iii) post-synthesis impregnation of MIL-100(Fe) with an aqueous solution of the heteropolyanion.

Experimental section

Synthesis

Synthesis of MIL-100(Fe)noF (noF stands for no fluorine). A mixture of $FeCl_3 \cdot 6H_2O$ (1mmol, 162.2 mg) and trimethyl 1,3,5-benzenetricarboxylate (0.66 mmol, 138,7 mg) dispersed in 5 mL of water was heated for three days at 130 °C in a Teflon lined autoclave. Then, the orange solid was recovered by filtration, washed with acetone and dried under air. Yield: 47%.

Direct synthesis of $PMo_{12}O_{40}^{3-}$ in the presence of MIL-100(Fe)noF. 100 mg of MIL-100(Fe)noF (100 mg of orange-pink solid) was added under stirring into an aqueous solution composed of 1.45 g of $Na_2MoO_4 \cdot 2H_2O$, 170 mL of water and 3.4 mL of H_3PO_4 (0.14 mol L^{-1}). The pH was adjusted to 1.8 by the addition of concentrated H_2SO_4 resulting in a yellowish solution. The UV-visible spectrum of the filtrate indicates the presence of $[PMo_{12}O_{40}]^{3-}$ ions. After different contact times (from 2 h to 16 h), the solid was recovered and washed with distilled water until a colourless filtrate was obtained. Then, the solid was dried with ethanol and ether and then collected by centrifugation. Due to dissolution of the MOF with time, 80 mg of solid was collected after one hour against a smaller amount, 40 mg, after 16 h. In order to estimate the influence of pH on the aqueous stability of MIL-100(Fe)noF, a suspension of MIL-100(Fe)noF was acidified up to pH 1.8 by adding concentrated H_2SO_4. After one hour, the solid was recovered by centrifugation (15000 rpm, 5 min) and characterized by IR.

Synthesis of MIL-100(Fe) in the presence of $H_3PMo_{12}O_{40}$, denoted H_3PMo_{12}@MIL-100(Fe)noF. $FeCl_3 \cdot 6H_2O$ (1.89g) was dissolved into a solution of $H_3PMo_{12}O_{40}$ (3.15 g) in 50 mL of water. Then triethyl 1,3,5-benzenetricarboxylate (1.36 g) was added. The mixture was heated for three days at 130 °C in a Teflon lined autoclave. Then, the orange solid was recovered by filtration and washed with ethanol and ether.

Synthesis of MIL-100(Fe) in the presence of $Na_6P_2Mo_{18}O_{62}$. $FeCl_3 \cdot 6H_2O$ (1.89 g) was dissolved into a solution of $Na_6P_2Mo_{18}O_{62}$ (4.43 g) in 50 mL of water. Then triethyl 1,3,5-benzenetricarboxylate (1.36 g) was added. The mixture was heated for three days at 130 °C in a Teflon lined autoclave. Then, the orange solid was recovered by filtration and washed with ethanol and ether.

Impregnation

Impregnation of MIL-100(Fe)noF with $Na_2HPMo_{12}O_{40}$. 1 g of MIL-100(Fe)noF was suspended in 100 mL of water. After the addition of 400mg of $Na_2HPMo_{12}O_{40}$ the slurry was stirred at room temperature for 20 h (pH = 2.6). The solid was collected by filtration, and washed several times with distilled water until a colourless filtrate was obtained. 1 g of solid were recovered and is designed hereafter as Na_2HPMo_{12}/MIL-100(Fe)noF

Impregnation of MIL-100(Fe)noF with $H_3PMo_{12}O_{40}$. 0.1 g of MIL-100(Fe)noF was suspended in 10 mL of water. After the addition of 40 mg of $H_3PMo_{12}O_{40}$ the slurry was kept under stirring at room temperature for 5 h. The solid was collected by filtration, and washed several times with distilled water until a colourless filtrate was obtained. 45 mg of solid were recovered.

Instrumentation

X-Ray powder diffraction (XRPD) patterns were recorded at room temperature with a Siemens D 5000 diffractometer using Cu $K_{\alpha 1,2}$ radiation (λ = 1.54059, 1.54439 Å).

X-Ray thermodiffractometry (XRTD) was performed under air in an Anton Paar HTK16 high temperature device of a Siemens D 5000 diffractometer (θ–θ mode) using Co K_α radiation (λ = 1.7903 Å), and equipped with a M Braun linear position sensitive detector (PSD). Samples were deposited directly on the heating platinum support connected to a thermocouple. Patterns were recorded from 20 °C to 430 °C every 10 °C, with a temperature ramp of 1.8 °C min^{-1}. The temperature was stabilized 2 min before every measurement; each data collection lasted 570 s.

Thermogravimetric analyses (TGA) were carried out under air (60 mL min^{-1}) with a Perkin-Elmer electrobalance TGA-7 at a heating rate of 5 °C min^{-1} up to 600 °C. Infrared spectra of KBr pellets were recorded on a Fourier transform Nicolet 550 apparatus.

The ^{31}P NMR spectra were recorded on a Bruker DSX-300 spectrometer operating at 121.51 MHz, with a classical 4 mm probe head allowing spinning rates up to 10 kHz. The chemical shifts are given relative to 85% H_3PO_4 (external reference, precision 0.5 ppm). As the recycle delay can be very high in crystalline POMs, this parameter was carefully checked. If for the pure heteropolyacid T1 was of some seconds, it was very short (less than 0.1 s) for the polyacid entrapped in the MOF. The chemical shift anisotropy was determined by using DMFIT and spectra recorded at low spinning rates.

^{57}Fe Mössbauer spectra were recorded in transmission geometry using a conventional acceleration spectrometer and a ^{57}Co source diffused into a rhodium matrix. The sample consists of a thin layer of powder containing 15 mg Fe while the experimental conditions are detailed above. Both the velocity and isomer shift values were calibrated using an α-Fe foil at 300 K. Mössbauer spectra were recorded at 77 K.

Bright field TEM, HAADF-STEM and EELS experiments were performed on a JEOL 3000F TEM/STEM microscope operated at 300 kV and equipped with a GIF-2000 post-column spectrometer. The EELS experiments were carried out in diffraction mode using a convergence semi-angle α of 0.9 mrad, a collection semi-angle β of 1.8 mrad, an energy dispersion of 0.3 eV per pixel and an energy resolution of approximately 1.2 eV. All core-loss spectra were background subtracted, aligned using the onset of the carbon peak (at 283 eV), deconvoluted using the zero-loss peak and normalized in intensity to their maxima. The HAADF-STEM images were taken with an approximate inner ADF detector semi-angle of 40 mrad.

Results and discussion

POM insertion into porous MIL-100(Fe) solid was investigated using several methods: direct synthesis, *in situ* formation of the POM within preformed MIL-100(Fe) and, finally, post-synthesis loading of the POM. Then, the stability towards leaching of the different solids was evaluated.

Direct synthesis of POM loaded MIL-100(Fe)

In order to achieve a direct synthesis of a POM loaded MIL-100(Fe) solid, the conditions reported for MIL-100(Fe) had to be considered first. This used hydrothermal conditions and a mixture of iron metal, trimesic acid, hydrofluorhydric acid and nitric acid leading to a fluorinated MIL-100(Fe) sample, denoted here as HF-MIL-100(Fe).[8] In the present case, the presence of iron metal was of high concern due to the potential reduction of the phosphomolybdates. Thus, other synthesis conditions had to be defined. Using iron chloride $FeCl_3 \cdot 6H_2O$ and an ester of trimesic acid (trimethyl 1,3,5-benzenetricarboxylate) in water at 130 °C for three days (see experimental section), a crystalline non-fluorinated material, denoted MIL-100(Fe)noF, was obtained as confirmed by X-ray powder diffraction (Fig. 1). This new route offers many advantages in comparison to the previously reported method: i) a faster synthesis (three days compared to seven), ii) avoids the use of corrosive acids (HF, HNO_3), iii) $FeCl_3$ as iron source to circumvent the reduction of phosphomolybdates in the presence of Fe^0. Please note that the direct use of trimesic acid under such conditions only leads to poorly crystalline solids. Thus, the substitution of 1,3,5-benzenetricarboxylic acid (1,3,5-BTC) by trimethyl benzenetricarboxylate allowed a better control of the reaction kinetics through the slow hydrolysis of ester moieties, leading to a well crystalline MIL-100(Fe) solid.

Elemental analysis of MIL-100(Fe)noF, based on the structure formula $Fe^{III}_3O(OH)(H_2O)_2\{C_6H_3(CO_2)_3\}_2 \cdot nH_2O$ ($n \sim 14.6$), is in agreement with the theoretical values with Fe and C contents of 19.6% and 26.4% (calc.: 19.1% Fe, 24.6% C), respectively, despite a slight excess of the carbon content due to the presence of residual free acid. No chlorine was found in the solid (% Cl < 200 ppm), indicating that the counteranion is here probably a OH group. Thermal gravimetric analysis of MIL-100(Fe)noF (Fig. 2) is in agreement with the formula $Fe_3O(OH)(H_2O)_2[C_6H_3(CO_2)_3]_2 \cdot 18H_2O$. Hydration water molecules (≈30%) leave the structure before 140 °C while the collapse of the framework occurs through the departure of the benzenetricarboxylic acid (46%) between 250 and 400 °C resulting in Fe_2O_3 at higher temperatures.

Using the synthesis conditions of MIL-100(Fe)noF, the direct synthesis of MIL-100(Fe)noF in the presence of Keggin phosphomolybdate ($H_3PMo_{12}O_{40}$) or Dawson molybdophosphate ($Na_6P_2Mo_{18}O_{62}$) was carried out (see experimental). Note that Dawson molybdophosphates are usually decomposed into the more stable Keggin structure under hydrothermal conditions. In both cases, a crystalline orange solid is obtained, and the structure is confirmed by powder X-ray diffraction (Fig. 1).

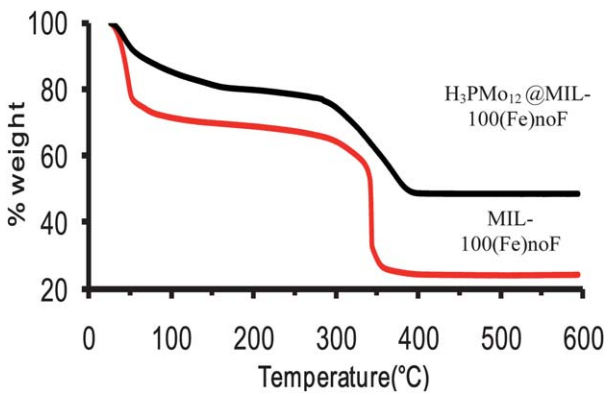

Fig. 2 TGA under air (2 °C min^{-1} heating rate) of MIL-100(Fe)noF and MIL-100(Fe) (grey) synthesized in the presence of $H_3PMo_{12}O_{40}$ (black).

UV-visible spectroscopy and IR analysis confirm that both direct syntheses lead to the same product: a $H_3PMo_{12}O_{40}$ entrapped within MIL-100(Fe)noF, denoted H_3PMo_{12}@MIL-100(Fe)noF. EDX confirms the absence of sodium cations in this solid. Interestingly, the Keggin structure of the phosphomolybdate is maintained, as confirmed by IR spectroscopy and solid state ^{31}P NMR, while the MIL-100 structure is formed.

Although the positions of XRPD Bragg peaks of H_3PMo_{12}@MIL-100(Fe)noF are similar to those of MIL-100(Fe)noF, a strong change in relative intensities, especially at low angles, is observed, in agreement with a significant change in the electronic density within the pores of MIL-100(Fe). The same phenomenon was previously observed for MIL-101(Cr) loaded with Keggin ions.[4]

Elemental analysis (Table S1†) of H_3PMo_{12}@MIL-100(Fe)noF indicates a remarkable loading capacity of POM (Mo/Fe = 0.95), close to *ca.* 65 POM per unit cell (containing 816 Fe). As one unit cell contains 8 large and 16 small mesoporous cages, one can estimate approximately 22 POM molecules for the 8 large cages and 43 for the 16 small cages considering that POMs occupy both cages with the same filling ratio. However, considering the van der Waals diameter of Keggin moieties (~13 Å) and the size of each cage (24 and 29 Å), small cages are likely to accommodate only one POM per cage while larger ones might accommodate about six POMs per cage (see Scheme S1†). This is in agreement with a maximum theoretical occupancy within the large cages of six POMs per cage.

TG analyses of MIL-100(Fe)noF and H_3PMo_{12}@MIL-100(Fe)noF are displayed in Fig. 2. As expected, H_3PMo_{12}@MIL-100(Fe)noF exhibits a lower weight loss than MIL-100(Fe)noF. A first weight loss up to 80 °C corresponds to the departure of free water molecules, while water molecules in stronger interaction with the framework and/or POM moieties leave between 80 and 200 °C. One can note the smaller water content in the POM containing MIL-100(Fe)noF (~9 water molecules per formula unit instead of 18 for MIL-100(Fe)noF) due to the occupancy of the cages by POM. Finally, the solid degrades at higher temperature (>270 °C) with the departure of the benzenetricarboxylate groups (2.5 observed against 2 theoretical per formula unit).

Elemental analysis confirms the presence of an excess of organic linker (theoretical and experimental C/Fe ratio 6 and 8.1, respectively), which represents 0.5 linker molecules per formula unit. This means that the current activation process using water, ethanol and ether was not sufficient enough in the case of the H_3PMo_{12}@MIL-100(Fe)noF solid. It is also likely that the presence of POM within the pores makes the diffusion of the linker out of the pores harder.

The thermal behaviour was followed by X-ray thermodiffraction (Fig. S1†). XRD patterns of MIL-100(Fe)noF show an increase of the intensity of low angle diffractions up to around 60 °C, as a consequence of dehydration. The structure remains unchanged up to 310 °C when the structure starts to degrade, with a totally amorphous phase observed at 370 °C. Upon heating at 410 °C a large peak appears at $2\theta = 27.8°$, indicating the crystallisation of iron oxide. H_3PMo_{12}@MIL-100(Fe)noF patterns show a different relative intensity of the Bragg diffraction peaks in comparison to MIL-100(Fe), as already observed above. The structure remains stable up to 320 °C, remarking a slight modification of the intensity of some peaks from 230 °C. Then, formation of crystalline $Fe_2(MoO_4)_3$ occurs at 390 °C. This ferric molybdate has been typically prepared from Fe_2O_3 and MoO_3 at 800 °C[16] or by oxidation of $FeMoO_4$ at 450–550 °C.[17] This decrease in the formation temperature of $Fe_2(MoO_4)_3$ could be explained by the dispersion and confinement effect of POM inside MIL-100(Fe).

Nitrogen sorption–desorption isotherms and pore size distribution are shown in Fig. 3. The pore volume and surface area ($S_{Langmuir}$) decrease from 0,882 to 0,373 $cm^3\ g^{-1}$ and from ~2800 to ~1000 $m^2\ g^{-1}$ for MIL-100(Fe)noF and H_3PMo_{12}@MIL-100(Fe)noF, respectively, in agreement with the presence of heavy phosphomolybdate moieties. According to the elemental analysis, the contribution of POM moieties to the molar weight of H_3PMo_{12}@MIL-100(Fe)noF reaches 65 wt%. Therefore, the surface area of the H_3PMo_{12}@MIL-100(Fe)noF, not taking into consideration the increase in density due to the POM loading, would reach 1500 $m^2\ g^{-1}$, in total agreement with the presence of an important residual porosity despite the Keggins. This is of great importance for the catalytic applications of POM inserted into porous MOFs since diffusion of the reactants is required. Estimation of the pore size distribution by the Horvath–Kawazoe method shows two maxima at 15 and 20.8 Å for MIL-100(Fe)noF, attributed to small and large cages, respectively. Note that the values are underestimated in comparison to van der Waals diameters calculated from crystalline structure (XRPD).

For H_3PMo_{12}@MIL-100(Fe)noF, no homogeneous pore size distribution is observed. This is consistent with the formation of heterogeneous pockets of different sizes as a consequence of the POM. These pockets are nevertheless accessible to the nitrogen gas. This is an important feature since diffusion of reactant could be possible for catalysis.

IR spectroscopy characterisation (Fig. 4) reveals additional bands in the H_3PMo_{12} containing MIL-100(Fe)noF corresponding to molybdophosphate at 1059, 958, 872 and 814 cm^{-1} attributed to $\nu_{as}(P–O_a)$, $\nu_{as}(Mo{=}O_d)$, $\nu_{as}(Mo–O_b)$ and $\nu_{as}(Mo–O_c)$, respectively. The $\nu_{as}(P–O_a)$ and $\nu_{as}(Mo–O_c)$ vibration bands are remarkably shifted in comparison to free molybdophosphate (1068 and 790 cm^{-1}, respectively). This shift discloses the confinement effect of POM inside the porous solid. Additionally, the band at 1544 cm^{-1} in MIL-100(Fe)noF disappears while a vibration band appears at 1710 cm^{-1} ($\nu_{as}(C{=}O)$) and 1280 cm^{-1} ($\nu(C–O)$), in agreement with the presence of free benzenetricarboxylic acid, as evidenced by elemental analysis.

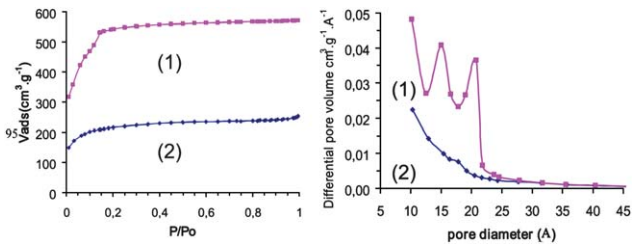

Fig. 3 Nitrogen sorption–desorption isotherms at 78 K (P_0 = 1 atm) (left) and Horvath–Kawazoe pore distribution (right) of MIL-100(Fe)noF (1) and MIL-100(Fe) synthesised in the presence of $H_3PMo_{12}O_{40}$ (2).

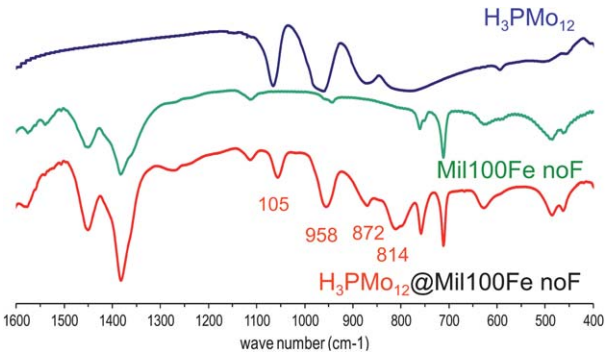

Fig. 4 IR spectra of $H_3PMo_{12}O_{40}$, MIL-100(Fe)noF and H_3PMo_{12}@MIL-100(Fe)noF.

Fig. 5 shows the solid-state ^{31}P MAS NMR spectrum of $H_3PMo_{12}O_{40}$ H_3PMo_{12}@MIL-100(Fe)noF compared to that of the free heteropolyacid. Clearly the spectrum of the incorporated heteropolyacid is similar to that of the bulk compound, with a similar chemical shift. However a careful analysis of the data reveals that (i) the chemical shift anisotropy (as deduced from simulations of the curves obtained at low spinning rates) has increased from less than 10 ppm to *ca.* 90 ppm and (ii) the T1 relaxation rate has considerably decreased compared to the bulk compound, being lower than 0.2 s. The unchanged chemical shift indicates that the integrity of the Keggin unit is kept inside MIL-100(Fe), in agreement with IR data. The increase in the chemical shift anisotropy shows that the interaction between the MIL-100(Fe) framework and Keggin polyanion is weak, as expected for ionic bonds, and is supported by surrounding phosphorus, in agreement with a low mobility of the Keggin unit within the mesoporous cages. The presence of bulk heteropolyacid can be excluded as deduced from the shorter relaxation time, in agreement with the recent work of Zhu *et al.*[18]

Mössbauer spectra recorded at 77 K on both MIL-100(Fe)noF and H_3PMo_{12}@MIL-100(Fe)noF samples are illustrated in Fig. 6. It is important to emphasize that they were first obtained at both 77 K and 300 K with a large velocity scale (not shown here): the presence of only a quadrupolar feature allows us to unambiguously conclude that no magnetic iron oxide or hydroxide occurs as impurity. Then Mössbauer experiments were performed with a bath cryostat, *i.e.* the as-prepared powdered sample at atmospheric pressure (Fig. 6a), then with a cryo-furnace, *i.e.* the as-prepared powdered sample under vacuum (Fig. 6b) and finally, *in situ* after a 1 h treatment at 70 °C (under vacuum) to check whether H_2O molecules were located within pores (Fig. 6c). From the shape of the spectra, the main changes are observed on MIL-100(Fe)noF suggesting that more H_2O molecules are entrapped within the pores during the synthesis and the natural ageing of the sample. In contrast, the adsorption of H_2O molecules is limited by the presence of polyoxometalate in the case of H_3PMo_{12}@MIL-100(Fe)noF. This could mean POM partially occupies some free volume within the cages. The exact modelling of the hyperfine structure remains rather difficult because of the lack of resolution. The asymmetrical quadrupolar doublets have to be described by means of at least three quadrupolar components, the proportions of which are dependent on the fitting conditions (constraints on linewidth and/or intensity), in agreement with previously reported results for fluorinated MIL-100(Fe).[8] The values of isomer shift clearly indicate the presence of high spin Fe^{3+} ions located in octahedral units, with different anionic environments. A decrease of the mean isomer shift (which is independent of the fitting model) is observed for the different tested conditions (from atmospheric pressure to 70 °C under vacuum: 0.54 down to 0.51 and 0.51 down to 0.47 mm s^{-1} relative to α-Fe for MIL-100(Fe)noF and H_3PMo_{12}@MIL-100(Fe)noF, respectively) while the mean quadrupolar splitting value is significantly reduced in the case of MIL-100(Fe)noF. The slight decrease of the isomer shift from 0.51 to 0.47 mm s^{-1} in the presence of POM indicates a perturbation of the environment of Fe^{3+} as a consequence of the presence of POM inside the cages of MIL-100(Fe)noF.

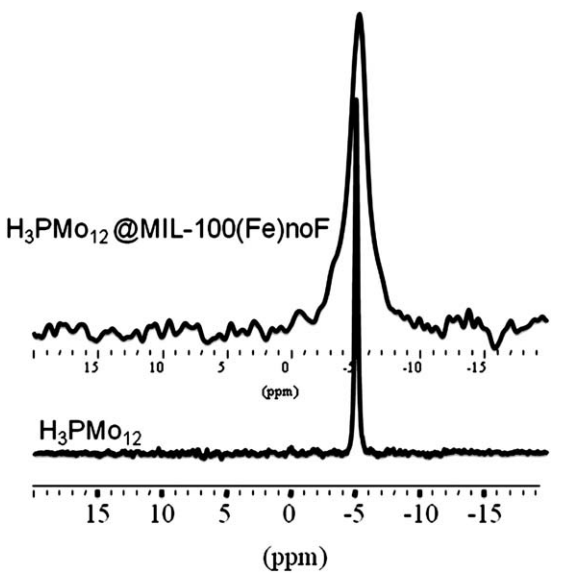

Fig. 5 ^{31}P MAS NMR at a spinning rate of 10 kHz for $H_3PMo_{12}O_{40}\cdot 13H_2O$ and H_3PMo_{12}@MIL-100(Fe)noF.

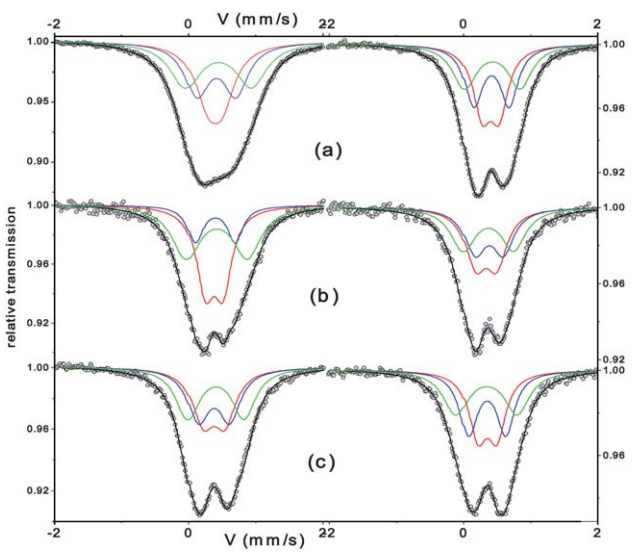

Fig. 6 Evolution of Mössbauer spectra recorded on MIL-100(Fe)noF (left) and H_3PMo_{12}@MIL-100(Fe)noF (right) powdered samples at 77 K at atmospheric pressure (a), under vacuum (b) and after *in situ* 1 h treatment at 70 °C (c).

It is of interest to analyse what are the potential driving forces for the incorporation of POM within the pores of MIL-100(Fe)noF. This porous iron tricarboxylate exhibits a cationic framework, compensating the one negative charge per iron trimer with anions such as hydroxyl or fluorine (MIL-100(Fe)noF or MIL-100(Fe)). Thus, are POMs hosted in MIL-100 in their acidic, neutral or anionic forms? Considering charge balance, two hypotheses can be raised: i) a cationic MIL-100(Fe)noF loaded with heteropolyanions (Scheme S1b†) or (ii) a neutral heteropolyacid hosted in the neutral MIL-100(Fe)noF form (Scheme S1a†).

On the one hand, IR analysis of MIL-100(Cr) previously indicated the presence of hydroxyl groups as a part of the framework, in addition to the coordinated fluorine atoms.[19] In our case, no fluorine is present, and one could postulate that one OH and two H_2O groups are coordinated to each iron trimer, which is also consistent with a higher polarizing of Fe^{3+} compared to Cr^{3+} and with the lack of chlorine in the MIL-100(Fe)noF. Considering a neutral mesoporous framework, one could propose the following formula here for H_3PMo_{12}@MIL-100(Fe)noF: $\{Fe_3O(H_2O)_2OH[C_6H_3(CO_2)_3]_2\}[H_3PMo_{12}O_{40}]_{0.2375}$-$[C_6H_3(CO_2C_2H_5)_3]_{0.5}\cdot 9H_2O$. On the other hand, according to the strong acidity of heteropolyacids, the reaction occurs at pH $\sim$ 2 and it is likely that the POM exhibits an anionic $PMo_{12}O_{40}^{3-}$ form solvated by water molecules to produce $H_5O_2^+$ cations.[20] Both ionic species could be encapsulated inside the neutral mesoporous cavities. The ionic model cannot be completely ruled out, since no sodium was present in the final material unless it was introduced with the starting POM, like $Na_6P_2Mo_{18}$. In this case the most suitable formula for H_3PMo_{12}@MIL-100(Fe)noF is the one where heteropolyanions moieties compensate positive charges of the hybrid solid: $\{Fe_3O(H_2O)_{2.71}(OH)_{0.29}[C_6H_3$-$(CO_2)_3]_2\}[PMo_{12}O_{40}]_{0.2375}[C_6H_3(CO_2C_2H_5)_3]_{0.5}\cdot 9H_2O$.

POM species are then hosted in the MOF governed by weak interactions (van der Waals, electrostatic…) but strong enough ionic interactions between anionic POM and the cationic MOF, as proposed previously for the immobilization of POM in positively charged modified mesoporous silica.[21]

The two models differ in the position of protons which can be easily delocalized with hydration water molecules. Thus ^{57}Fe Mossbauer spectrometry was used to evidence only slight differences between hydrated MIL-100(Fe)noF and POM containing MIL-100(Fe)NoF. However, after treatment at 70 °C under vacuum, a smaller decrease of the mean isomer shift and a significant reduction of the mean quadrupolar splitting value are observed in the case of MIL-100(Fe)noF. Thus, dehydration has less effect on the iron coordination sphere of the sample with POM. We have to consider the effect of dehydration in the two models. If the protons are incorporated on the iron trimer (cationic framework) the hydrogen bonding with water molecules could be replaced by hydrogen bonding with the oxygen atoms of dehydrated POM. This is in agreement with a change in the color of H_3PMo_{12}@MIL-100(Fe)noF which turns from pale orange to greenish-brown upon heating ($T > 70$ °C). Thus, it can be assumed that the removal of coordinated water[9] possibly leads to a coordination of iron Lewis acid sites with oxygen atoms of POM. In the case of a neutral framework, dehydrated heteropolyacid should be formed and hydrogen bonding of the hydroxo ligand of iron will be removed by dehydration like for the pure MIL-100(Fe)noF.

Other loading methods

Finally, other methods of producing a POM-MIL-100(Fe) solid were investigated. First, *in situ* synthesis of $[PMo_{12}O_{40}]^{3-}$ in the presence of MIL-100(Fe)noF was attempted. A suspension of the MOF into a solution of $Na_2MoO_4\cdot 2H_2O$ and H_3PO_4 under acidic conditions (pH = 1.8) was stirred at room temperature. After one hour, the solution became yellowish, characteristic of phosphomolybdate, as confirmed by UV-visible spectroscopy. However, the yellow colour could also be attributed to Fe^{3+} in solution due to degradation of the iron carboxylate MOF. The IR spectrum showed a decrease of the band at 1710 cm^{-1} and additional weak and large bands in comparison to MIL-100(Fe)noF at 1040, 877 and 807 cm^{-1}, similar to those observed in the MIL-100(Fe)noF solid alone acidified for one hour at pH 1.8. This confirms the partial destruction of the solid at low pH. In this case the 1040 cm^{-1} band cannot be assigned to P–O vibrations which are observed as an intense and sharp band at 1060 cm^{-1}, quite independent of the nature of the counter-ion of the 12-molybdophosphate. Solid degradation was estimated as 24.4% by dosing the concentration of trimesic acid in the solution by HPLC. Moreover, the total amount of suspended solid drastically decreases after 16 h, in agreement with the dissolution of the solid. Consequently, the low stability of MIL-100(Fe)noF under the acidic conditions (pH = 1.8), which are needed for the *in situ* formation of $[PMo_{12}O_{40}]^{3-}$, rules out the use of *in situ* synthesis of POM within the pores of MIL-100(Fe).

In a last step, impregnation of MIL-100(Fe)noF with an aqueous solution of $H_3PMo_{12}O_{40}$ was carried out, knowing that the size of the windows of MIL-100(Fe) will prevent any adsorption within the pores and allow adsorption of POM only at the external surface of the particles. After impregnation, a partial degradation of the MOF is observed due to the acidic pH of the POM solution (pH = 1.8). Again, IR characterisation of the impregnated solid shows the decrease of the band at 1710 cm^{-1} and the presence of additional weak bands at 1040, 877 and 807 cm^{-1} due to the degradation under acidic conditions. To reduce the degradation of the solid, impregnation of MIL-100(Fe)noF with the less acidic $Na_2HPMo_{12}O_{40}$ was carried out (pH = 2.6). Only a very low proportion of POM was adsorbed on the external surface (Mo/Fe ratio = 0.14) corresponding roughly to ~9.5 POM per unit cell containing 816 Fe, as estimated by elemental analysis. The Na/POM ratio after analysis was found to be 1.75, comparable to the initial $Na_2HPMo_{12}O_{40}$ (Na/POM ratio = 2) and confirming the presence of the salt and possibly a small fraction of deprotonated POM. IR characterisation again shows a new band at 1540 cm^{-1} and weak bands at 1060, 870 and 813 cm^{-1}, in agreement with a small content of POM. Similarly, IR bands comparable to those observed with the H_3PMo_{12}@MIL-100(Fe)noF solid obtained by direct synthesis are observed, indicating that the POM moieties exhibit a strong interaction with the surface of the particles. XRPD confirm the integrity of the MIL-100(Fe) structure, even though additional diffraction peaks at 2θ = 9.5, 14.4 and 28.5° (which were not present in H_3PMo_{12}@MIL-100(Fe)noF) appear. Note that the relative Bragg peak intensities are similar to those of MIL-100(Fe)noF, in concordance with the location of the $Na_2HPMo_{12}O_{40}$ on the external surface and not into the pores (Fig. S2†). Nitrogen sorption–desorption isotherms and pore size distribution are

illustrated in Fig. S3.† The pore volume and surface area decrease from 0.882 to 0.543 $cm^3\ g^{-1}$ and from $S_{Langmuir}$ ~2800 to ~1600 $m^2\ g^{-1}$, for MIL-100(Fe)noF to Na_2HPMo_{12}/MIL-100(Fe)noF, respectively. The pore size distribution established by the Horvath–Kawazoe method gives evidence for two maxima at 15 and 20.8 Å as for MIL-100(Fe)noF, attributed to small and large cages, respectively. The decrease in surface area is only due to the increase of weight due to the presence of heavy POM since POM can only be located on the external surface.

Stability tests

In order to assess the stability of the POM-MIL-100(Fe)noF, solids made following the various methods described above compared to the pure MIL-100(Fe)noF solid and solid impregnated by Na_2HPMo_{12} were dispersed into water. After two months in aqueous solution (Fig. 7), macroscopic direct observation of the solids did not reveal any change in colour for the MIL-100(Fe)noF and H_3PMo_{12}@MIL-100(Fe)noF solids.

However, microaggregates of greenish colour (black in Fig. 7) are visible from the Na_2HPMo_{12}/MIL-100(Fe)noF suspension. EDX analysis confirms that while the greenish aggregates region contains mainly Mo and Na (Mo/Fe ratio up to 5), the remaining domains contain mainly Fe (Mo/Fe ~ 0.14, which cannot be exactly compared to results from elemental analysis). Bearing in mind the high solubility of $Na_2HPMo_{12}O_{40}$, the formation of a new salt can be proposed. The partial decomposition of MIL-100(Fe) in acidic media may provide trimeric iron species such as $\{Fe_3O(H_2O)_3[C_6H_3(CO_2)_3]_6\}^+ \equiv (Fe_3)^+$ that can form $(Fe_3)^+Na_2PMo_{12}O_{40}$ salts similar to those reported by the group of Mizuno with chromium.[22]

In contrast, EDX analysis of H_3PMo_{12}@MIL-100(Fe)noF after two months in water did not show any change in composition, confirming the absence of any POM leaching. Furthermore, POM exchange tests using tetrabutylammonium perchlorate species in organic media did not lead to any $H_3PMo_{12}O_{40}$ replacement. This indicates that the POMs encapsulated by direct synthesis inside the cages of MIL-100(Fe)noF are stable, in agreement with the size of the windows being smaller than those of the POM.

Finally, H_3PMo_{12}@MIL-100(Fe)noF was stable after inmersion in different organic solvents (acetonitrile, chloroform and dimethylformamide) under stirring for 5 days at room temperature.

Electron microscopy analysis

Samples H_3PMo_{12}@MIL-100(Fe)noF, Na_2HPMo_{12}/MIL-100(Fe)noF and MIL-100(Fe)noF were also investigated by transmission electron microscopy, high-angle annular dark field scanning transmission electron microscopy (HAADF-STEM) and electron energy-loss spectroscopy (EELS) (Fig. 8). The EELS spectra were all collected from several pieces of loaded or unloaded MIL material. All EELS spectra show the presence of carbon, oxygen and iron through the carbon K-edge at 285 eV, the oxygen K-edge at 532 eV and the Fe $L_{2,3}$-edge at 708 eV. Sample H_3PMo_{12}@MIL-100(Fe)noF clearly shows the presence of Mo through the Mo M-edge starting at ~230 eV (first onset indicated by *, $M_{4,5}$ and $M_{2,3}$ indicated by arrows). Comparison of our EELS data with reference data from literature indicates that the molybdenum in sample H_3PMo_{12}@MIL-100(Fe)noF

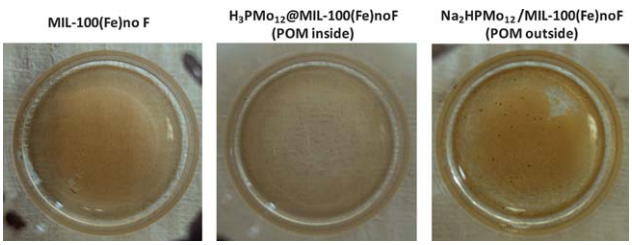

Fig. 7 Images of aqueous solutions of MIL-100(Fe)noF, H_3PMo_{12}@MIL-100(Fe)noF or Na_2HPMo_{12}/MIL-100(Fe)noF after two months.

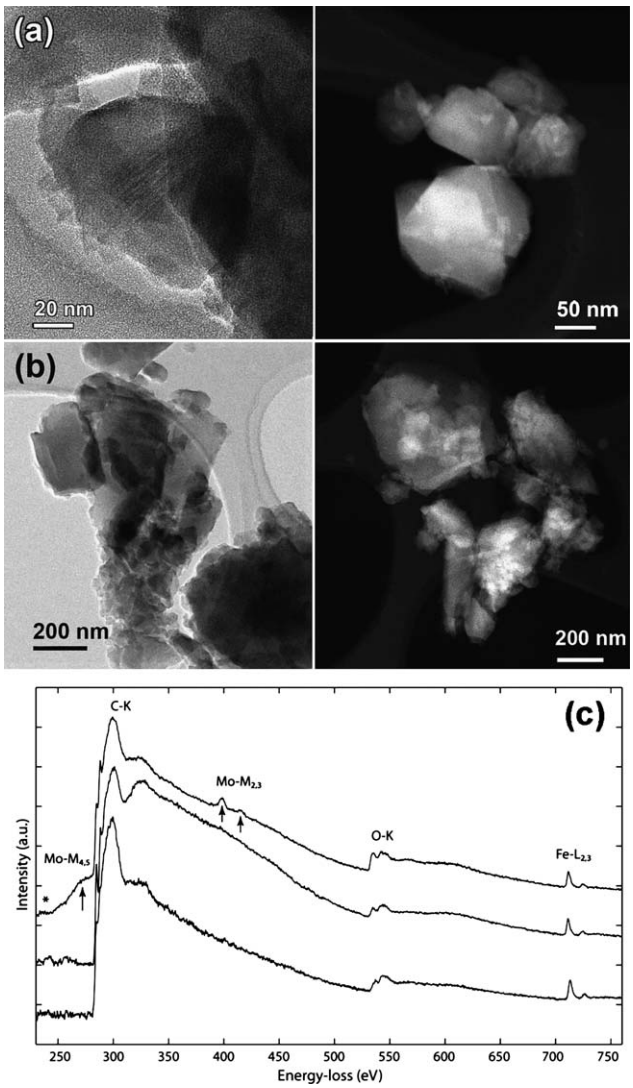

Fig. 8 (a) TEM (left) and HAADF-STEM (right) images of sample H_3PMo_{12}@MIL-100(Fe)noF; (b) TEM and HAADF-STEM images of sample Na_2HPMo_{12}/MIL-100(Fe)noF; (c) background subtracted, normalised EELS spectra of samples H_3PMo_{12}@MIL-100(Fe)noF (top), Na_2HPMo_{12}/MIL-100(Fe)noF (middle) and MIL-100(Fe)noF (bottom). All spectra show the presence of carbon, oxygen and iron through the carbon K-edge at 285 eV, the oxygen K-edge at 532 eV and the Fe $L_{2,3}$-edge at 708 eV. H_3PMo_{12}@MIL-100(Fe)noF shows the clear presence of Mo through the Mo M-edge starting at ~230 eV (first onset indicated by *, $M_{4,5}$ and $M_{2,3}$ indicated by arrows).

(top of Fig. 8c) is in an oxidized state, as pronounced $M_{2,3}$ white lines should not be present in the case of metallic Mo.[23–25] Although determination of the oxidation state of Mo is in principle possible *via* the fine structure of the Mo-M and O–K edges, this is not possible in the current samples due to a complex overlapping of the C–K and Mo-M edges and the fact that the O–K edge also arises from oxygen bound within the MIL host framework. The lowered Mo content in sample Na_2HPMo_{12}/MIL-100(Fe)noF makes detection *via* EELS difficult; no significant Mo $M_{4,5}$ edge is present at 270 eV, although a heightened contribution around 400 eV does appear to indicate the presence of Mo *via* the $M_{2,3}$ edge.

The bright field TEM images in Fig. 8 show typical H_3PMo_{12} loaded (a) and Na_2HPMo_{12} impregnated (b) MIL-100 framework crystals. In both samples the MIL-100 crystals show a large degree of faceting and have sizes ranging from ~30 to several hundred nanometres, in agreement with the particle size distribution determined by light diffusion scattering (DLS). The bright field TEM images in both cases are strikingly similar—the contrast over a single MIL-100 crystal is uniform and no large agglomerates can be discerned in the TEM images for sample H_3PMo_{12}@MIL-100(Fe)noF or sample Na_2HPMo_{12}/MIL-100(Fe)noF, a first indication that the POM clusters are well-dispersed in both samples. However, the very low amount of molybdenum in Na_2HPMo_{12}/MIL-100(Fe)noF does not allow us to detect any difference of contrast. According to the high molybdenum content in H_3PMo_{12}@MIL-100(Fe)noF, one could conclude that the POM dispersion is uniform in the whole material. This conclusion is corroborated by HAADF-STEM (*Z*-contrast) imaging. As the image contrast in this regime is mass-thickness sensitive, larger agglomerates should light up in the HAADF-STEM images. As no such agglomerates or structures can be made out in the image in Fig. 8a, the POM clusters are thought to be extremely small (<1 nm) and evenly spread out in H_3PMo_{12}@MIL-100(Fe)noF.

Conclusion

Several routes for the development of POM loaded porous iron carboxylate MIL-100(Fe) have been investigated. The *in situ* formation of POM in the presence of preformed hybrid solid as well as the post-synthesis encapsulation of the Keggin within the preformed MIL-100(Fe) did not lead to satisfying results. Only direct synthesis of POM-MIL-100(Fe)noF using the Keggin heteropolyanion $H_3PMo_{12}O_{40}$ allowed the successful entrapment of a remarkable amount of POM up to one and six POMs per small or large mesoporous cage, respectively. Although the porosity is slightly reduced, a significant porosity is maintained after the loading ($\Delta S_{Langmuir} \sim 1000$ m^2 g^{-1} and $\Delta V_p \sim 0.373$ cm^3 g^{-1}), as required for future catalysis applications. Finally, Keggin entrapped within MIL-100(Fe)noF solid is remarkably stable with no POM leaching after 2 months in aqueous solution and no exchange by tetrabutylammonium perchlorate in organic media. This paves the way for future catalytic applications based on non-toxic and cheap POM based iron MOFs.

Acknowledgements

This work was supported by project Grant ANR-06-BLAN 60353-02 Methanox, Ministère Français de l'Enseignement Supérieur et de la Recherche and Research Ministry (MENESR) and CNRS (UMR 8180). Y.-K. H. and J.-S. C. acknowledge the financial support (KN-1037) of NRF funded by the Ministry of Education, Science and Technology of Korea and the financial support by the KICOS international collaboration program.

Notes and references

1 (*a*) Special issue on polyoxometalates, *Chem. Rev.*, 1998, **98**, 1, and references therein; (*b*) A. S. R. Müller, *Coord. Chem. Rev.*, 2003, **245**, 153.
2 G. Férey, *Chem. Soc. Rev.*, 2008, **37**, 191–241.
3 R. Yu, X.-F. Kuang, X. YuanWu, C.-Z. Lu and J. P. Donahue, *Coord. Chem. Rev.*, 2009, **253**, 2872.
4 G. Férey, C. Mellot-Draznieks, C. Serre, F. Millange, J. Dutour, S. Surblé and I. Margiolaki, *Science*, 2005, **309**, 2040.
5 (*a*) C.-Y. Sun, S.-X. Liu, D.-D. Liang, K.-Z. Shao, Y.-H. Ren and Z. Min Su, *J. Am. Chem. Soc.*, 2009, **131**, 1883; (*b*) G. Hundal, Y. K. Hwang and J.-S. Chang, *Polyhedron*, 2009, **28**, 2450.
6 B. Xiao, P. S. Wheatley, X. B. Zhao, A. J. Fletcher, S. Fox, A. G. Rossi, I. L. Megson, S. Bordiga, L. Regli, K. M. Thomas and R. E. Morris, *J. Am. Chem. Soc.*, 2007, **129**, 1203.
7 G. Férey, C. Serre, C. Mellot-Draznieks, F. Millange, S. Surblé, J. Dutour and I. Margiolaki, *Angew. Chem., Int. Ed.*, 2004, **43**, 6296.
8 P. Horcajada, S. Surblé, C. Serre, D.-Y. Hong, Y.-K. Seo, J.-S. Chang, J.-M. Grenèche, I. Margiolaki and G. Férey, *Chem. Commun.*, 2007, 2820.
9 J. W. Yoon, Y.-K. Seo,1, Y. K. Hwang, J.-S. Chang, H. Leclerc, S. Wuttke, P. Bazin, A. Vimont, M. Daturi, E. Bloch, P. L. Llewellyn, C. Serre, P. Horcajada, J.-M. Grenèche, A. E. Rodrigues and G. Férey, *Angew. Chem., Int. Ed.*, 2010, in press.
10 P. L. Llewellyn, S. Bourrelly, C. Serre, A. Vimont, M. Daturi, L. Hamon, G. De Weireld, J.-S. Chang, D.-Y. Hong, Y. K. Hwang, S. H. Jhung and G. Férey, *Langmuir*, 2008, **24**(14), 7245.
11 N. V. Maksimchuk, M. N. Timofeeva, M. S. Melgunov, A. N. Shmakov, Yu. A. Chesalov, D. N. Dybtsev, V. P. Fedin and O. A. Kholdeeva, *J. Catal.*, 2008, **257**, 315.
12 J. Juan-Alcañiz, E. V. Ramos-Fernandez, U. Lafont, J. Gascon and F. Kapteijn, *J. Catal.*, 2010, **269**, 229.
13 J. C. A. Boeyens, J. G. McDougal and J. van Smit, *J. Solid State Chem.*, 1976, 18191.
14 I. V. Kozhevnikov, *Catal. Rev.*, 1995, **37**, 311.
15 A. M. Khenkin, L. Weiner, Y. Wang and R. Neumann, *J. Am. Chem. Soc.*, 2001, **123**, 8531.
16 M. H. Rapposch, J. B. Anderson and E. Kostiner, *Inorg. Chem.*, 1980, **19**, 3531.
17 U. kersen and L. Holappa, *Appl. Phys. A: Mater. Sci. Process.*, 2006, **85**, 431.
18 K. Zhu, J. Hu, X. She, J. Liu, Z. Nie, Y. Wang, C. H. F. Peden and J. H. Kwak, *J. Am. Chem. Soc.*, 2009, **131**(28), 9715.
19 A. Vimont, J.-M. Goupil, J.-C. Lavalley, M. Daturi, S. Surblé, C. Serre, F. Millange, G. Férey and N. Audebrand, *J. Am. Chem. Soc.*, 2006, **128**, 3218.
20 R. Allman and H. D'Amour, *Z. Krist.*, 1973, 1.
21 H. Kim, J. C. Jung and I. K. Song, *Catal. Surv. Asia*, 2007, **11**, 114.
22 (*a*) A. Lesbani, R. Kawamoto, S. Uchida and N. Mizuno, *Inorg. Chem.*, 2008, **47**(8), 3349; (*b*) S. Uchida and N. Mizuno, *Chem.–Eur. J.*, 2003, **9**, 5850.
23 R. F. Egerton, *Electron energy-loss spectroscopy in the TEM*, Plenum Press, New York and London, 1996.
24 D. S. Su, *Anal. Bioanal. Chem.*, 2002, **374**, 732.
25 F. Hofer, *Ultramicroscopy*, 1987, **21**, 63.